BUTTERWORTH HEINEMANN

Effect of eccentricity and thermal boundary conditions on laminar fully developed flow in annular ducts

R. M. Manglik and P. P. Fang
Department of Mechanical, Industrial, and Nuclear Engineering, University of Cincinnati, Cincinnati, OH, USA

Numerical solutions for laminar, fully developed, forced convective heat transfer in ecccentric annuli are presented. With an insulated outer surface, two types of thermal boundary conditions have been considered: constant wall temperature (***T***), and uniform axial heat flux with constant peripheral temperature (***H1***) on the inner surface of the annulus; these are representative of many practical applications. Isothermal friction factors and Nusselt numbers for concentric annulus are in excellent agreement with previously reported results. Velocity and temperature profiles, and isothermal $f\mathrm{Re}$, Nu_{iT}, and $\mathrm{Nu}_{i,H}$ values for different eccentric annuli ($0 \leq \varepsilon^* \leq 0.6$) with varying aspect ratios ($0.25 \leq r^* \leq 0.75$) are presented. The eccentricity is found to have a strong influence on the flow and temperature fields. The flow tends to stagnate in the narrow section and has higher peak velocities in the wide section. This flow maldistribution is found to produce greater nonuniformity in the temperature field and a degradation in the average heat transfer. Also, results show that the ***H1*** condition sustains higher heat transfer coefficients relative to the ***T*** condition on the inner surface, except for very large eccentricity.

Keywords: Laminar forced convection; duct flows; heat exchangers

Introduction

Steady-state, laminar forced convection heat transfer in circular and concentric annular ducts has been studied quite extensively (Shah and London 1978; Kakaç et al. 1987). This reflects the fact that these geometries are found in many industrial heat exchangers. For example, the simplest form of a two-fluid heat transfer device is a double-pipe heat exchanger made up of two concentric circular tubes, thereby presenting circular and annular duct flow geometries. The annular channel in the heat exchanger may be concentric or eccentric. Quite often, the eccentricity stems from manufacturing tolerances and/or deformation in the service of a nominally concentric annular duct configuration. In this case, the eccentricity may tend to be small; however, in some applications, design and construction considerations may result in a large eccentricity. Typical examples of the latter are oil/gas drilling wells, polymer/plastic extruders, and nuclear reactors.

In most double-pipe heat exchanger applications, where an eccentric annular flow geometry may exist, two primary thermal boundary conditions are usually encountered. These are uniform wall temperature (***T***), or uniform wall heat flux (***H1***) on the inner surface with an insulated (adiabatic) outer surface. These conditions essentially represent the thermal boundaries in a two-fluid heat exchanger for the cases where the inner tube fluid undergoes phase-change (boiling or condensation), or the inner and outer fluid flows have the same capacity rates, respectively. The first case corresponds to the fundamental boundary condition of the third kind for doubly connected ducts, and the second case is a modification of boundary condition of the fifth kind. For a detailed explanation of these fundamental boundary conditions, the monograph by Shah and London (1978) may be referred. Laminar flow heat transfer results for these two practical flow situations do not appear to have been presented in the literature for eccentric annuli (Shah and London 1978; Shah and Bhatti 1987).

An extended study of fully developed laminar flows in concentric annular ducts with four fundamental boundary conditions was conducted by Lundberg et al. (1963). Based on their analytical results, Shah and London (1978) have tabulated friction factor and Nusselt number values for the boundary conditions of the first, second, and third kind for different radius (or aspect) ratios; the fourth and fifth kinds are identical for concentric annuli and can be evaluated from the first kind results. For the case with ***H1*** condition on the inner wall and insulated outer wall in a concentric annular channel, Capobianchi and Irvine (1992) have reported results for fully developed laminar flows of modified power-law fluids. Here, the Newtonian fluid solutions correspond to the results for low shear rates and a flow behavior index of unity. Herwig and Klemp (1988), and Moghadam and Aung (1990) have presented extended solutions that account for temperature-dependent fluid property variations.

Laminar forced convection heat transfer in eccentric annuli was first considered by Cheng and Hwang (1968), and Trombetta (1971). In the study by Trombetta, results for fundamental boundary conditions of the first, second, and fourth kind have been presented for different eccentricities and radius ratios. Cheng and Hwang considered the ***H1*** boundary condition on both walls of the annular duct. In a more recent work, Suzuki et al. (1991) have reported finite-difference solutions for thermal boundary condition

Address reprint requests to Dr. Raj M. Manglik, Department of Mechanical, Industrial, & Nuclear Engineering, University of Cincinnati, P.O. Box 210072, Cincinnati, OH 45221-0072 USA.

Received 6 December 1994; accepted 6 May 1995.

Int. J. Heat and Fluid Flow 16: 298–306, 1995
© 1995 by Elsevier Science Inc.
655 Avenue of the Americas, New York, NY 10010

0142–727X/95/$10.00
SSDI 0142–727X(95)00030-T

of the second kind. However, as pointed out by them, this condition (uniform axial and peripheral heat flux on the inner wall) is not usually obtained in most practical applications. A more relevant case is to consider the ***H1*** condition (uniform axial heat flux with constant peripheral wall temperature) on the inner wall attributable to the high thermal conductivity of the metallic tubing normally used in heat exchangers; this is addressed in the present study. Some of the earlier studies—Snyder and Goldstein (1965), Jonsson and Sparrow (1965), and Piercy et al. (1933), among others—focused only on the fully developed hydrodynamic problem.

As outlined above, this study presents numerical solutions for fully developed laminar flow heat transfer in eccentric annular channels. Two different thermal boundary conditions are considered on the inner surface (the outer surface being insulated), that are representative of the practical usage of two-fluid, double-pipe heat exchangers. The numerical solutions are obtained using finite-difference techniques. Friction factor and Nusselt number results are presented for a wide range of eccentricities and channel radius ratios. Variations in the local velocity and temperature fields are also presented to highlight the influences of the geometry and boundary conditions.

Mathematical formulation

Laminar flow in a straight eccentric annular duct bounded by an outer radius r_o and an inner radius r_i is considered. The origin of the cylindrical coordinate system is placed at the center of the inner cylinder, which is located off-center from the outer cylinder with an eccentricity ε, as shown in Figure 1, so that the outer cylinder surface is described by the shape function $R(\bar{\psi})$. The constant property, Newtonian fluid flow is both hydrodynamically and thermally fully developed, and axial conduction, viscous dissipation, and effects of body forces are ignored. These are reasonable considerations for most viscous liquid flows with large Pr, (Re·Pr), and (L/d_h) (Shah and London 1978; Manglik and Bergles 1994). With the outer cylinder surface being thermally adiabatic, two different thermal boundary conditions on the inner cylinder are considered: constant temperature (***T***) and constant axial heat flux but peripherally constant temperature (***H1***). The corresponding momentum and energy equations in the cylindrical coordinate system of Figure 1 are as follows:

$$\mu\nabla^2\bar{w} - (\bar{d}p/d\bar{x}) = 0 \tag{1}$$

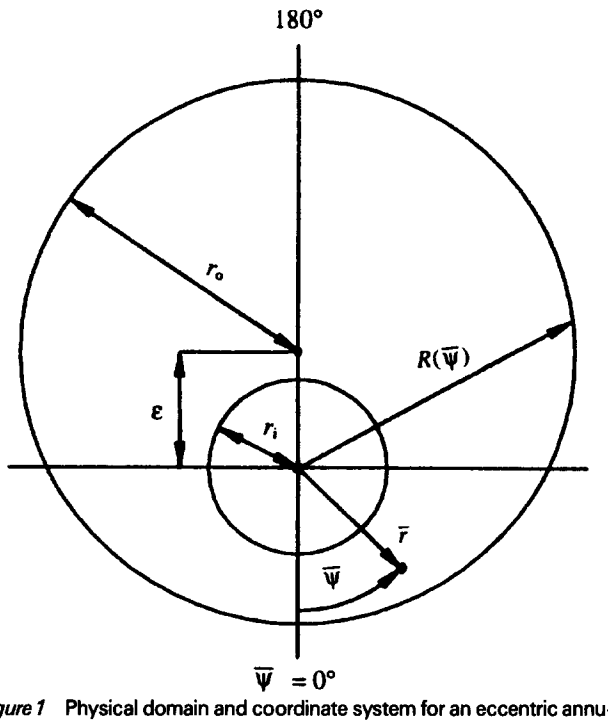

Figure 1 Physical domain and coordinate system for an eccentric annulus

$$\alpha\nabla^2\bar{T} - \bar{w}(\partial\bar{T}/\partial\bar{x}) = 0 \tag{2}$$

where

$$\nabla^2 = \frac{1}{\bar{r}}\frac{\partial}{\partial\bar{r}}\left[\bar{r}\frac{\partial}{\partial\bar{r}}\right] + \frac{1}{\bar{r}^2}\frac{\partial^2}{\partial\bar{\psi}^2}$$

and for thermally fully developed flows

$$\frac{\partial\bar{T}}{\partial\bar{x}} = \begin{cases} \left[\dfrac{\bar{T}_W - \bar{T}}{\bar{T}_W - \bar{T}_m}\right]\dfrac{d\bar{T}_m}{d\bar{x}} & \text{for } \boldsymbol{T} \quad (2a) \\ \dfrac{d\bar{T}_m}{d\bar{x}} & \text{for } \boldsymbol{H1} \quad (2b) \end{cases}$$

Notation

A_c	axial flow cross-sectional area, m^2
B	dimensionless shape function, Equations (4–6)
c_p	specific heat at constant pressure, kJ/(kg K)
d_h	hydraulic diameter, $=2(r_o - r_i)$, m
f	fanning friction factor $=(-dp/dx)d_h/(2\rho w_m^2)$
h	heat transfer coefficient, $W/(m^2\ K)$
H1	uniform axial heat flux with constant peripheral wall temperature boundary
k	fluid thermal conductivity, W/(m K)
Nu	hydraulic diameter based Nusselt number $=hd_h/k$
p	pressure, Pa
P_w	wetted perimeter, m
q''	average wall heat flux on the inner surface, w/m^2
Q_{wi}	dimensionless peripherally average heat flux on the inner surface, Equation 16
$\bar{r}$	radial coordinate, m
r	dimensionless radial coordinate $=(\bar{r} - r_i)/Br_o$, Equation 4
r^*	radius ratio of the annulus $=r_i/r_o$
R	shape function, Equation 5
Re	hydraulic diameter based Reynolds number $=\rho\bar{w}_m d_h/\mu$
T	constant wall temperature boundary
$\bar{T}$	local fluid temperature, K
T	dimensionless temperature, Equations 9a–b
$\bar{w}$	axial velocity, m/s
w	dimensionless axial velocity, Equation 8
$\bar{x}$	axial coordinate, m

Greek

α	thermal diffusivity, m^2/s
ε	eccentricity or displacement of inner cylinder, m
ε^*	dimensionless eccentricity $=\varepsilon/(r_o - r_i)$
μ	fluid dynamic viscosity, kg/m s
ρ	fluid density, kg/m^3
ψ	angular coordinate, rad

Subscripts

i	outer surface of inner cylinder
m	mean or bulk average
o	inner surface of outer cylinder
w	at the outer wall of inner cylinder

Equations 1 and 2 are subject to the following boundary conditions:

$$\bar{w} = 0, \bar{r} = r_i; \bar{w} = 0, \bar{r} = R(\bar{\psi}) \tag{3a}$$

$$\bar{T} = \bar{T}_W, \bar{r} = r_i; \frac{\partial \bar{T}}{\partial \bar{n}} = 0, \bar{r} = R(\bar{\psi}) \tag{3b}$$

The eccentric annular duct of Figure 1 can be mapped into a unit circle and rendered dimensionless by the following coordinate transformation (Prusa and Yao 1983):

$$r = \frac{\bar{r} - r_i}{B(\psi) r_o}, \psi = \bar{\psi} \tag{4}$$

Here, $B(\psi)$ is the dimensionless shape function that is defined as follows:

$$B(\psi) = (R(\psi) - r_i)/r_o \tag{5}$$

and for the eccentric annular shape it is given by the following:

$$B(\psi) = [1 - \varepsilon^{*2}(1 - r^*)^2 \sin^2 \psi]^{1/2} - \varepsilon^*(1 - r^*)\cos\psi - r^* \tag{6}$$

where

$$r^* = r_i/r_o, \varepsilon^* = \varepsilon/(r_o - r_i) \tag{7}$$

Also, the dimensionless velocity w and temperature T are defined as follows:

$$w = \bar{w}/[(-\mathrm{d}\bar{p}/\mathrm{d}\bar{x})d_h^2/\mu] \tag{8}$$

$$T = \begin{cases} \alpha(\bar{T}_W - \bar{T})/[\mathrm{d}_h^2 \bar{w}_m(\mathrm{d}\bar{T}_m/\mathrm{d}\bar{x})] & \text{for } \boldsymbol{T} \quad (9a) \\ (\bar{T}_W - \bar{T})/(q''\mathrm{d}_h/k) & \text{for } \boldsymbol{H1} \quad (9b) \end{cases}$$

Thus, the dimensionless form of the governing momentum and energy equations are

$$M_1 \frac{\partial^2 w}{\partial r^2} + M_2 \frac{\partial^2 w}{\partial \psi^2} + M_3 \frac{\partial^2 w}{\partial r \partial \psi} + 2\lambda \frac{\partial w}{\partial r} + S_{\phi 1} = 0 \tag{10}$$

$$M_1 \frac{\partial^2 T}{\partial r^2} + M_2 \frac{\partial^2 T}{\partial \psi^2} + M_3 \frac{\partial^2 T}{\partial r \partial \psi} + 2\lambda \frac{\partial T}{\partial r} + S_{\phi 2} = 0 \tag{11}$$

where

$$M_1 = \frac{1}{B^2} + \frac{r^2}{(Br + r^*)^2}\frac{B'^2}{B^2}, M_2 = \frac{1}{(Br + r^*)^2},$$

$$M_3 = -\frac{2r}{(Br + r^*)^2}\frac{B'}{B}$$

$$\lambda = \frac{1}{2}\left[\frac{1}{B(Br + r^*)} + \frac{r}{(Br + r^*)^2}\left(\frac{2B'^2}{B^2} - \frac{B''}{b}\right)\right]$$

$$S_{\phi 1} = \frac{1}{4(1 - r^*)^2}, \; S_{\phi 2} = \begin{cases} \dfrac{1}{4(1 - r^*)^2}\dfrac{w}{w_m}\dfrac{T}{T_m} & \text{for } \boldsymbol{T} \\ \dfrac{r^*}{(1 + r^*)(1 - r^*)^2}\dfrac{w}{w_m} & \text{for } \boldsymbol{H1} \end{cases}$$

Equations 10 and 11 are subject to the following boundary conditions:

$$w = 0, r = 0, 0 \le \psi \le 2\pi; w = 0, r = 1, 0 \le \psi \le 2\pi \tag{12a}$$

$$T = 0, r = 0, 0 \le \psi \le 2\pi; \frac{\partial T}{\partial n} = 0, r = 1, 0 \le \psi \le 2\pi \tag{12b}$$

Note that $B' = (\mathrm{d}B/\mathrm{d}\psi)$, and $B'' = (\mathrm{d}^2B/\mathrm{d}\psi^2)$ in the above expressions.

Given the velocity and temperature fields, the friction factor and the Nusselt number are the two global parameters of design interest that need to be evaluated. From a force balance across the flow cross section and its simplification, the hydraulic diameter based Fanning friction factor is given by

$$f\mathrm{Re} = 1/(2w_m) \tag{13}$$

The dimensionless mean flow velocity w_m can be calculated from its definition as

$$w_m = \frac{1}{\pi(1 - r^{*2})}\int_0^1 \int_0^{2\pi} wB(Br + r^*)\mathrm{d}\psi \, \mathrm{d}r \tag{14}$$

For the Nusselt number, the usual hydraulic diameter based definition is employed and

$$\mathrm{Nu} = \frac{hd_h}{k} = \begin{cases} (Q_{wi}/T_m) & \text{for } \boldsymbol{T} \\ (1/T_m) & \text{for } \boldsymbol{H1} \end{cases} \tag{15}$$

where the dimensionless heat flux on the inner cylinder Q_{wi} is given by

$$Q_{wi} = \frac{(1 - r^*)}{\pi}\int_0^{2\pi} \frac{1}{B}\frac{\partial T}{\partial r}\bigg|_{r=0} \mathrm{d}\psi \tag{16}$$

and the dimensionless bulk temperature T_m by

$$T_m = \frac{1}{\pi(1 - r^{*2})w_m}\int_0^1 \int_0^{2\pi} wTB(Br + r^*)\mathrm{d}\psi \, \mathrm{d}r \tag{17}$$

Thus, Equations 10–17 provide the complete formulation for the velocity and temperature fields and the corresponding f and Nu for eccentric annular ducts.

Numerical Solution

To obtain solutions for the partial differential equations that describe the velocity and temperature fields, finite-difference methods have been employed in this study. The finite differencing strategies that have been adopted essentially follow those of Prusa and Yao (1982) and Manglik and Bergles (1994). The transformed space for the flow field described by Equations 10 and 11 is divided into a mesh of radial lines intersecting circular arcs concentric with the boundary $r = 1$, with Nr radial nodes and Ns angular nodes. The nodes in the radial and angular directions have uniform spacing of Δr and $\Delta\psi$, respectively. For Equations 10 and 11, second-order accurate, centered differencing is employed for the radial and angular diffusion terms. The mixed derivative, $(\partial^2/\partial r \partial\psi)$, is also represented by a second-order scheme by employing double Taylor series expansions. The radial convective terms is represented by a modified central-difference scheme that incorporates upwind differencing with a correction term, and the second-order accuracy is essentially achieved by using both terms (Manglik and Bergles 1991).

All the boundary conditions for $w(r, \psi)$, and $T(r, \psi)$ are very straightforward Dirichlet conditions, with the exception of the adiabatic outer cylinder surface for the temperature field. Here zero heat flux is prescribed at the $r = 1$ boundary, and, in terms of the temperature gradient, it follows that

$$\left\{\left[\frac{1}{B} + \frac{r}{(Br + r^*)}\frac{B'^2}{B^2}\right]\frac{\partial T}{\partial r} - \frac{B'}{B(Br + r^*)}\frac{\partial T}{\partial \psi}\right\}_{r=1} = 0 \tag{18}$$

Consequently, the local wall temperature can be calculated by employing a second-order representation of the first derivatives (Anderson et al. 1984). Furthermore, to calculate the peripherally averaged wall heat flux from Equation 16, the derivative for the wall gradient was represented by a three-point second-order scheme.

The finite-difference equations for the velocity and temperature fields were solved by the Gauss–Seidel, point-iterative scheme

Table 1 Comparison of friction factor and Nusselt number results for fully developed laminar flow in concentric annuli

	fRe		Nu_{iT}		Nu_{iH1}	
r^*	Present study	Shah and London (1978)	Present study	Shah and London (1978)	Present study	Capobianci and Irvine (1992)
0.00	———	16.000	———	∞	———	———
0.05	21.564	21.567	17.317	17.460	17.709	———
0.10	22.342	22.343	11.474	11.560	11.865	11.938
0.25	23.302	23.302	7.343	7.371	7.728	———
0.30	23.461	23.461	6.828	———	7.218	7.274
0.40	23.679	23.678	6.148	———	6.563	6.588
0.50	23.811	23.813	5.733	5.738	6.162	6.185
0.60	23.896	23.897	5.443	———	5.894	5.915
0.70	23.949	23.949	5.229	———	5.704	5.723
0.75	23.967	23.967	5.146	———	5.593	———
0.90	23.995	23.996	4.950	———	5.422	5.681
0.95	23.998	23.999	4.899	———	5.377	———
1.00	———	24.000	———	4.861	———	5.387

along with the use of SOR. An overrelaxation factor of $\omega = 1.4$ was employed for all computations. The iterative convergence was established when the relative error in the dependent variable between two successive iterations was less than 10^{-6} throughout the computational domain. For the temperature solution, it was necessary to apply underrelaxation to the adiabatic wall temperatures in order to obtain stable and convergent solutions; a factor of $\omega = 0.8$ was used. The average axial velocity and the bulk mean temperature were determined by numerical integration using the Simpson's rule (combination of 3/8 and 1/3 rules). Also, the peripherally average heat flux for the T condition, given by Equation 16, was obtained by a heated-surface-area averaged summation of the wall derivatives.

The grid size is very important to the convergence and accuracy of the solutions, especially when the radius ratio is small, and the eccentricity is large. In the present study, the accuracy and the concomitant grid refinement were established by comparing the results for concentric annular ducts with those reported in the literature. This is given in Table 1, where results for (fRe), $Nu_{i,T}$, and $Nu_{i,H1}$ are presented. Here, the (fRe) and $Nu_{i,T}$ values given by Shah and London (1978) are from analytical solutions; the $Nu_{i,T}$ values are based on the solution of Lundberg et al. (1963). The $Nu_{i,H1}$ results of Capobianchi and Irvine (1992) are from a finite-difference solution. As can be seen from Table 1, excellent accuracy is established in the present results (the maximum deviatio in the present values is less than 1%). These were obtained with grid sizes ranging from 21 × 61 to 61 × 61, with the finer mesh used for the small radius ratio ducts. The same mesh size was used to generate the eccentric annular duct results. In these cases, starting from a course mesh, grid refinement was effected till the change in the numerical results for (fRe) was less than 1%. However, it may be noted that for very small radius ratio and very large eccentricity, the mapping of the duct geometry by $R(\psi)$ results in a lack of orthogonality in the coordinate system. Consequently, some numerical errors will exist for these extreme cases no matter how refined a grid is used.

Results and discussion

Numerical results for both local variables (w and T) and global paramerers (fRe and Nu) are presented for eccentric annular ducts. These reflect the influence of the eccentricity and aspect ratio of the annulus on the flow field, as well as the effect of thermal boundary conditions on the convective transport. Several different duct geometries have been considered with $0 \le \varepsilon^* \le 0.6$ and $0.25 \le r^* \le 0.75$, which is representative of many practical applications.

Velocity and temperature field

The eccentricity of an annular duct geometry has a strong influence on the laminar flow velocity distribution. This is seen in Figure 2, where the dimensionless axial velocity profiles, normalized by the mean velocity, are presented for $r^* = 0.5$ and $0 \le \varepsilon^* \le 0.6$. As eccentricity increases, the flow velocity tends to have a sharper profile with higher gradients and peak velocities in the widest end of the annulus ($\psi = 180°$). At the narrowest end ($\psi = 0°$), on the

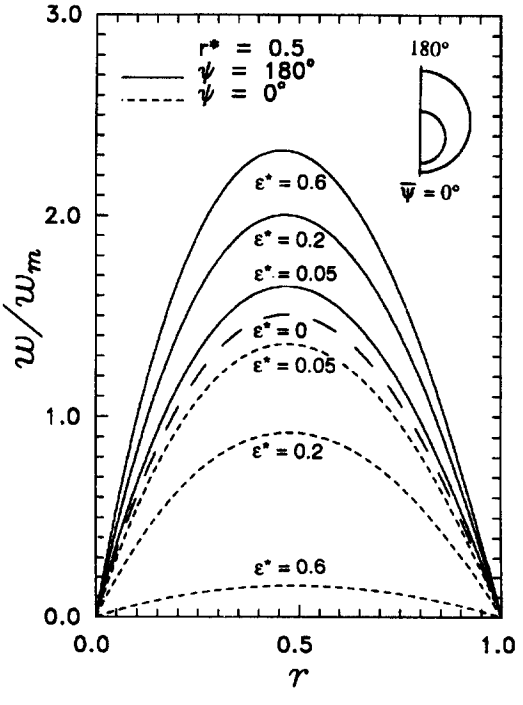

Figure 2 Effect of eccentricity on radial distribution of axial velocity in the widest and narrowest gap of annulus

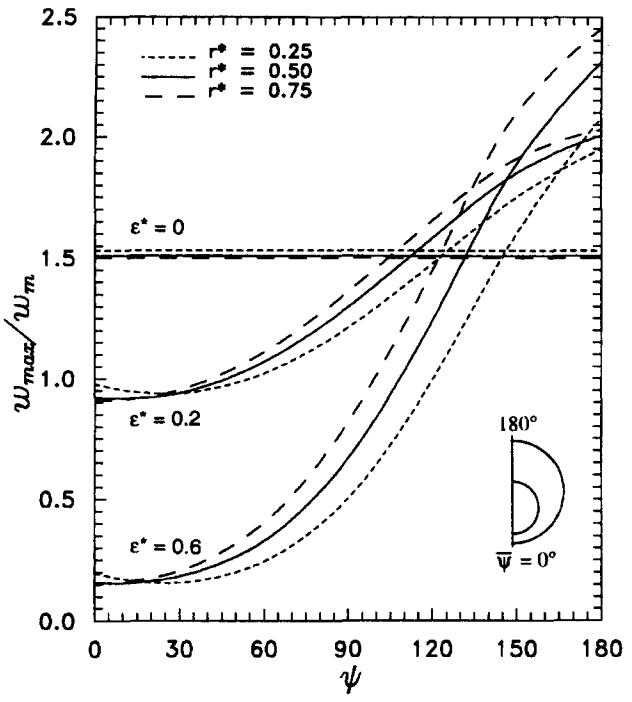

Figure 3 Influence of eccentricity and aspect ratio on the peak flow velocity distribution around the annulus

other hand, the channel restriction causes the peak velocity to decrease drastically, and the flow becomes effectively immobile for $\varepsilon^* > 0.6$. In fact, the angular distribution of the relative magnitude of the peak velocities $[w_{max}/w_m(\psi)]$ can be considered as a measure of local fluid mobility around the annulus. This is illustrated in Figure 3, where the variations in (w_{max}/w_m) with ψ for $r^* = 0.25$, 0.50, and 0.75, and $\varepsilon^* = 0$, 0.2, and 0.6 in each case are given. In a concentric annulus $\varepsilon^* = 0$, the peak axial velocity is constant. However, for the case of $r^* = 0.5$ and $\varepsilon^* = 0.2$, for example, (w_{max}/w_m) is 33.3% higher in the wide side and 38.7% lower in the narrow side of the annulus, relative to the concentric duct. These values change to 54% and 89.7%, respectively, when $\varepsilon^* = 0.6$; the narrow section's flow blockage results in higher velocities in the wider annular gap.

Two different thermal boundary conditions have been considered in this study: (1) constant temperature (*T*) on the inner surface and adiabatic outer surface (boundary condition of the 3rd kind); and (2) constant axial heat flux with constant peripheral temperature (*H1*) on the inner surface and adiabatic outer surface (modified 5th kind boundary condition). The effect of eccentricity of the annular duct on the temperature profiles for these two cases is illustrated in Figure 4a and 4b, respectively. Dimensionless temperature profiles $T(r)/T_m$ are presented for $r^* = 0.5$ and $\varepsilon^* = 0$, 0.05, 0.2, and 0.6 at $\psi = 0°$ and 180°. With higher velocities in the wider gap of the annulus, there are sharp temperature gradients in the flow; whereas, the almost stagnant fluid in the narrow gap tends to uniformly attain the inner wall temperature as ε^* increases. However, with increasing ε^*, the temperature gradients tend to

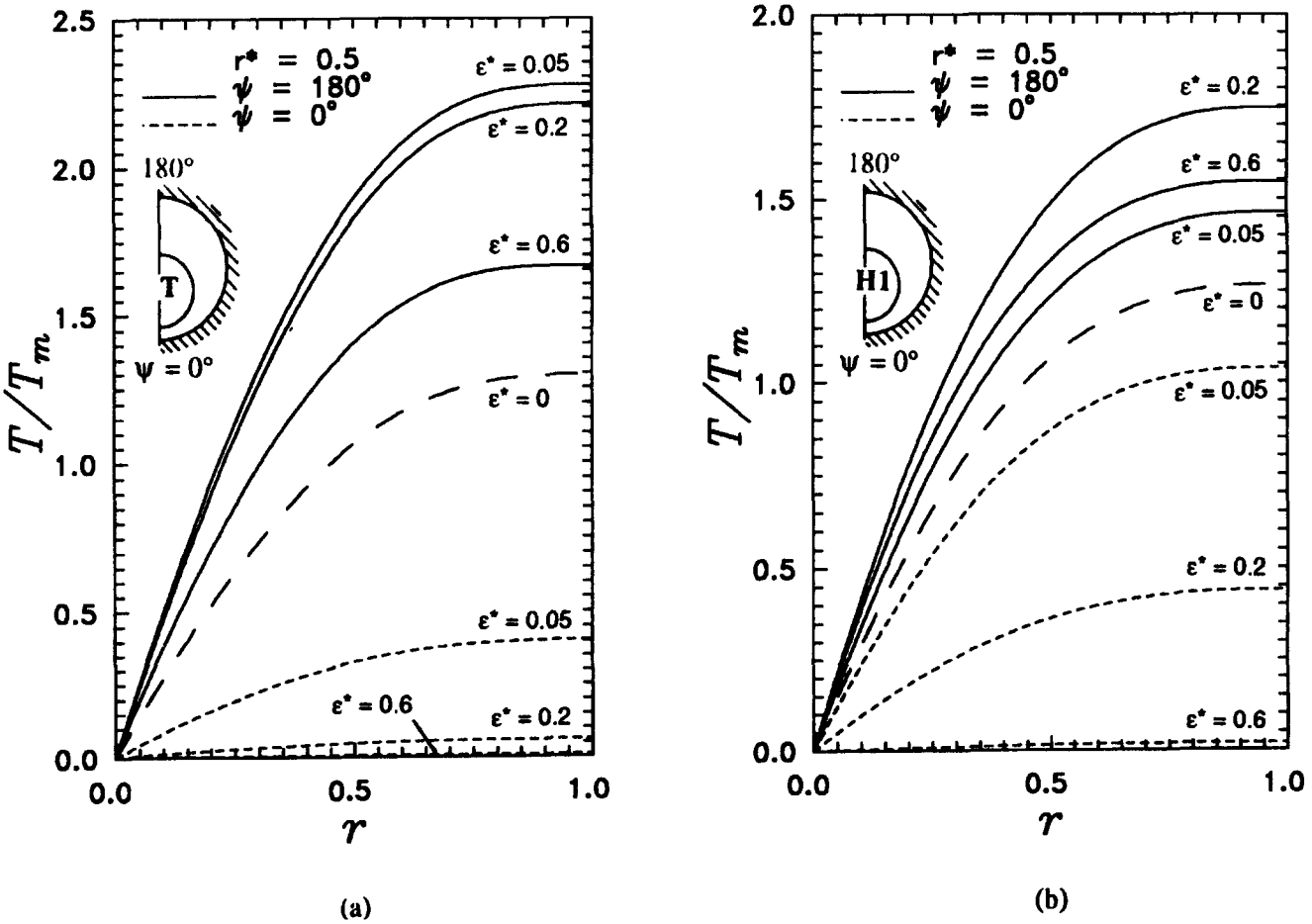

Figure 4 Effect of eccentricity on the radial variation of temperatuere in the widest and narrowest gap: (a) *T* condition, and (b) *H1* condition on the inner wall

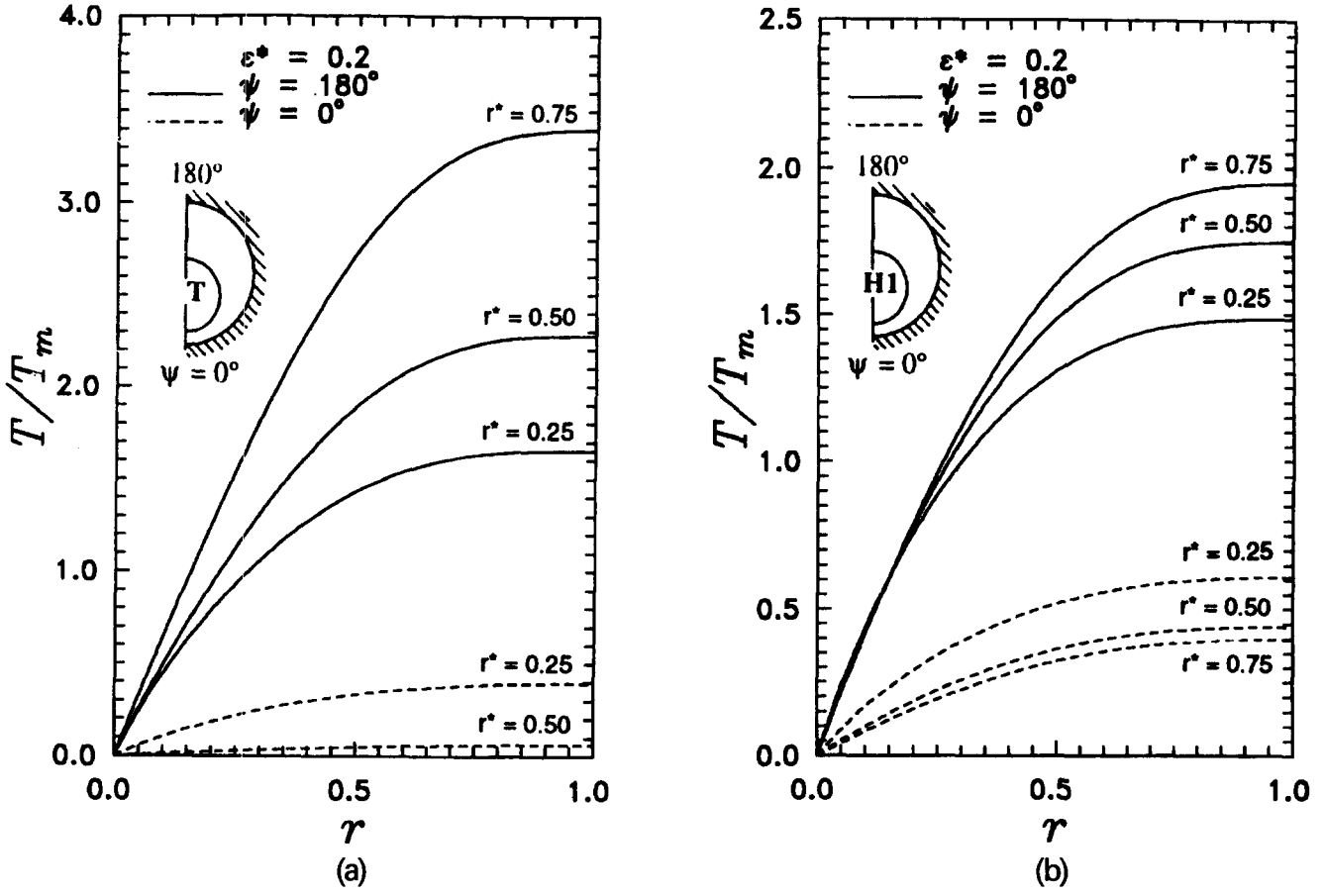

Figure 5 Effect of annulus aspect ratio on the radial variation of temperature in the widest and narrowest gap: (a) ***T*** condition, and (b) ***H1*** condition on the inner wall

decrease over most sections around the annulus, reflecting the worsensing heat transfer behavior. In the widest gap ($\psi = 180°$), initially with small eccentricity ($\varepsilon^* \sim 0.05 - 0.2$), the temperature gradient tends to increase, but reduces drastically for larger ε^*, as seen from Figure 4. The ***H1*** condition tends to sustain this trend for slightly higher eccentricity ($\varepsilon^* \sim 0.2$) relative to the ***T*** condition (optimum at $\varepsilon^* \sim 0.05$); the constant heat flux case generally produces higher heat transfer coefficients in duct flows. The correponding effects of aspect ratio of the duct are evident in Figure 5, where the radial temperature distribution for $\varepsilon^* = 0.2$ and $r^* = 0.25$, 0.50, and 0.75 at $\psi = 0°$ and 180° are presented. With large values of r^*, even a small eccentricity has a strong influence on the temperature field. In fact, while the temperature gradient increases sharply with increasing r^* in the widest gap, it is more than negated by the large detioration in the narrowest gap of the annulus.

Increasing the eccentricity ε^* and reducing the radius ratio r^* of the annulus geometry results in large nonuniformities in the axial velocity and temperature fields. This is clearly evident from Figures 6 and 7, where the isovelocity and isothermal contours for several different cases and the two boundary conditions are presented. Figure 6 shows the effect of eccentricity ($r^* = 0.5$, $\varepsilon^* = 0$, 0.05, and 0.6) on the fluid flow and temperature distribution around the annulus, and Figure 7 shows the influence of the aspect ratio of the duct geometry ($r^* = 0.25$, 0.5, and 0.75, with $\varepsilon^* = 0.2$). As can be seen from these figures, with a moderate aspect ratio ($r^* = 0.5$) of the annulus, even a small degree of eccentricity produces significant distortions in both the velocity and temperature fields. The flow tends to stagnate in the narrow sections of the annulus and "squeeze" higher flow velocities in the wider sections. Thermally, the ***T*** boundary condition on the inner wall results in greater asymmetries in the temperature distribution around the annulus, as compared with the ***H1*** condition. In both cases, however, local hot or cold regions are generated in the flow field with sharp differences in local temperature gradients. This flow maldistribution and inhomogeneity in the temperature field is particularly detrimental in thermal-processing applications in the food and chemical industry; such conditions would lead to excessive thermal degradation of the fluid product. The thermal maldistribution is enhanced even more significantly when the aspect ratio increases in a moderately eccentric annulus ($\varepsilon^* = 0.2$, Figure 7).

Friction factor and Nusselt number

Given the velocity and temperature distributions, the respective friction factor and Nusselt number values are the results of primary design interest. As indicated earlier, a wide variation in the aspect ratio ($0.25 \le r^* \le 0.75$) and eccentricity ($0 \le \varepsilon^* \le 0.6$) of the annulus geometry has been considered in this study. The corresponding results for $f\mathrm{Re}$, $\mathrm{Nu}_{i,\mathbf{T}}$ and $\mathrm{Nu}_{i,H1}$ are presented in Table 2.

The isothermal friction factor results can be compared with the values tabulated by Shah and London (1978); the latter are based on the analytical solutions of Piercy et al. (1933) and Tiedt (1966, 1967). As can be seen from Table 2, there is excellent agreement between these results and those obtained in the present study. There is, however, some deviation for large values of $\varepsilon^*(\ge 0.6)$,

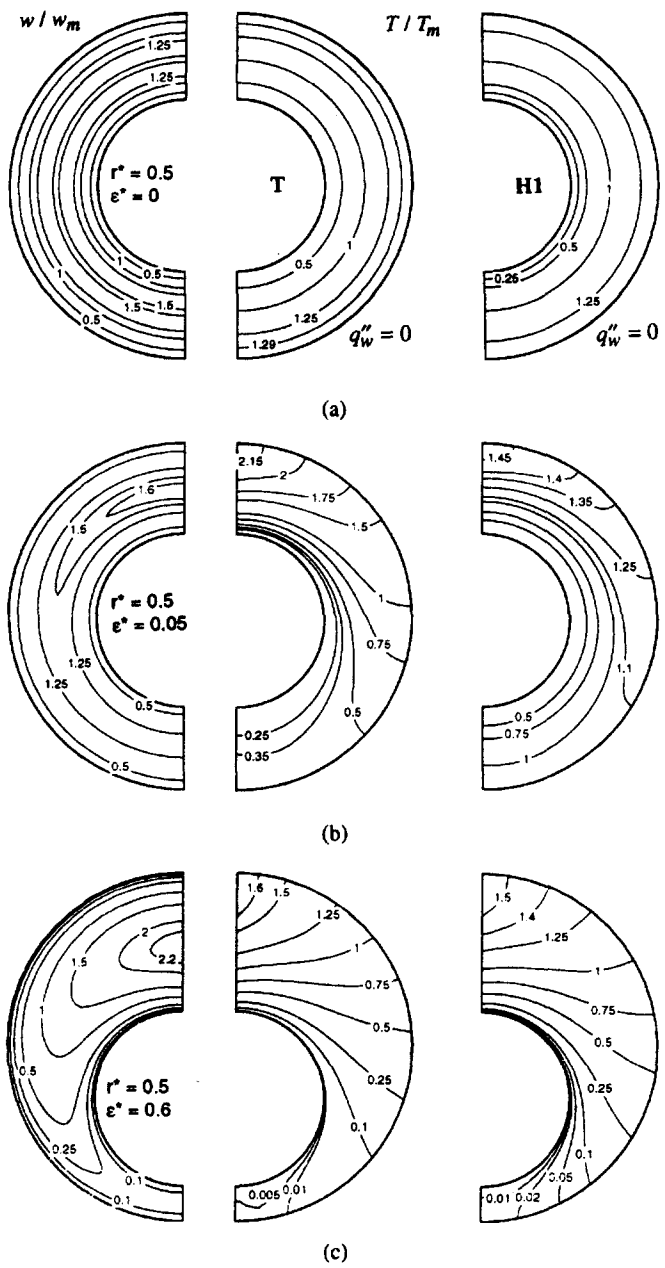

Figure 6 Isovelocity and isothermal contour maps for $r^* = 0.5$ and ***T*** and ***H1*** boundary conditions on the inner wall: (a) $\varepsilon^* = 0$, (b) $\varepsilon^* = 0.05$, and (c) $\varepsilon^* = 0.6$

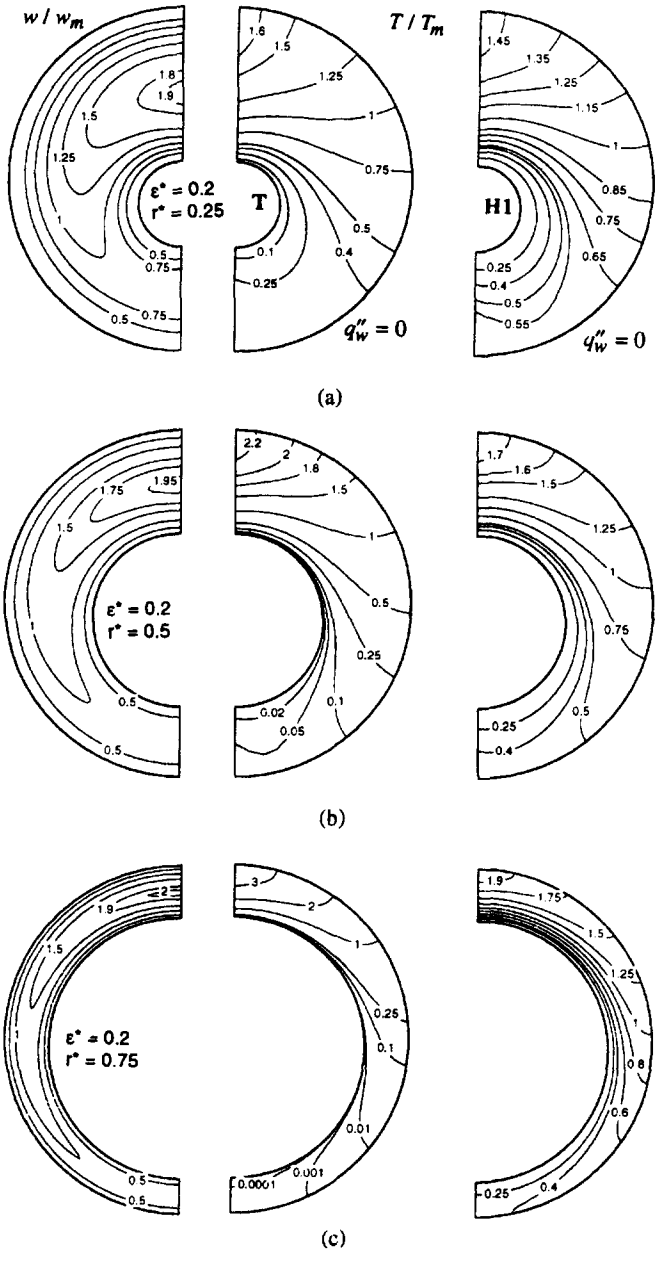

Figure 7 Isovelocity and isothermal contour maps for $\varepsilon^* = 0.2$ and ***T*** and ***H1*** boundary conditions on the inner wall: (a) $r^* = 0.25$, (b) $r^* = 0.5$, and (c) $r^* = 0.75$

particularly when $r^* \leq 0.4$. As has been pointed out in the previous section, this is attributable to the nonorthgonality of the mapping coordinate system at these extreme conditions. Nevertheless, the results illustrate the varying influences of ε^* and r^*. For $\varepsilon^* < 0.4$, the fRe values increase monotonically as r^* increases and tend to attain almost constant values for $r^* \geq 0.6$. On the contrary, for $\varepsilon^* \geq 0.4$, the fRe values tend to decrease considerably with increasing r^*. Sharp reduction in friction factor occurs when the eccentricity is large in annuli with small radius ratios, $0.1 \leq r^* \leq 0.5$. Although not presented here, this decrese is even greater for $\varepsilon^* \geq 0.7$ (Shah and Bhatti 1987).

From the Nusselt number results tabulated in Table 2, the effects of the thermal boundary condition on the inner surface and the eccentricity and aspect ratio of the annular duct are evident. It is observed that the Nusselt number generally decreases with increasing values of ε^* and r^*. Also, the ***H1*** boundary condition sustains higher heat transfer coefficients compared to the ***T*** boundary condition. Because the wall temperature is higher and "runs away" from the bulk fluid temperature with the ***H1*** condition, higher wall temperature gradients, and, hence, higher heat transfer coefficients are obtained; with the ***T*** condition, the bulk temperature approaches the wall temperature as the flow becomes fully developed. This difference, however, is significant only for small to moderate eccentricities, and it reverses for large ε^* in small diameter ratio ($r^* \leq 0.5$) ducts. For example, with $r^* = 0.4$ and $\varepsilon^* > 0.4$, the $\mathrm{Nu}_{i,\mathbf{T}}$ value approaches an asymptotic constant ($\mathrm{Nu}_{i,\mathbf{T}} \cong 2.8$) which is higher than the corresponding value for $\mathrm{Nu}_{i,\mathbf{H1}} (\cong 2.36)$. Once again, these anomalies are primarily

Table 2 Isothermal friction factor and Nusselt numbers for fully developed laminar flow in eccentric annuli.

		fRe		Nu_{iT}	Nu_{iH1}
r^*	ε^*	Present study	Shah and London (1978)	Present study	Present study
0.75	0.00	23.967	23.967	5.146	5.593
	0.05	23.877	23.878	4.483	5.485
	0.20	22.603	22.625	2.947	4.304
	0.40	19.309	19.375	1.979	2.768
	0.60	15.540	15.646	1.524	1.936
0.60	0.00	23.896	23.897	5.443	5.884
	0.05	23.805	23.811	4.916	5.772
	0.20	22.521	22.587	3.370	4.549
	0.40	19.213	19.415	2.355	2.930
	0.60	15.446	15.770	1.887	2.061
0.50	0.00	23.811	23.813	5.733	6.162
	0.05	23.720	23.729	5.306	6.048
	0.20	22.423	22.541	3.760	4.788
	0.40	19.094	19.458	2.709	3.113
	0.60	15.322	15.909	2.244	2.194
0.40	0.00	23.679	23.678	6.148	6.552
	0.05	23.585	23.598	5.825	6.436
	0.20	22.265	22.465	4.307	5.157
	0.40	18.894	19.515	3.223	3.387
	0.60	15.095	16.107	2.806	2.362
0.25	0.00	23.302	23.302	7.343	7.728
	0.05	23.203	23.231	7.143	7.606
	0.20	21.809	22.234	5.778	6.204
	0.40	18.267	19.615	4.769	4.081
	0.60	14.295	16.558	4.998	2.605

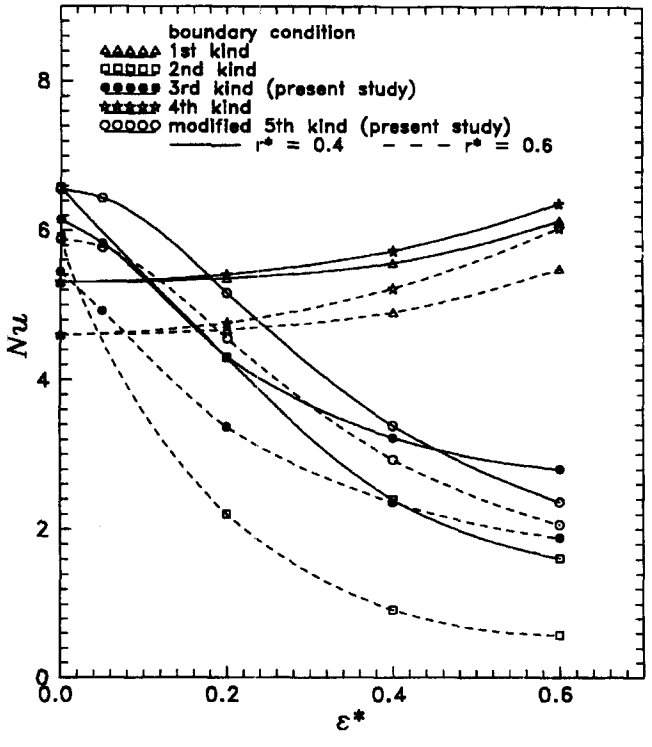

Figure 8 Comparison of Nusselt number result of present study with those for fundamental boundary conditions of 1st, 2nd, and 4th kind (from Shah and London 1978)

attributable to the flow maldistribution and consequent distortions in the temperature field around the annulus as ε^* increases and r^* decreases.

A comparison of the present Nu results (boundary conditions of the 3rd and modified 5th kind) with those for boundary conditions of the 1st, and 4th kind (Shah and London 1978) is given in Figure 8. In all cases, except with the 1st and 4th kind, the Nusselt number decreases with increasing eccentricity for a given r^*; in the other two cases, Nu increases. Furthermore, the results for ***T*** and ***H1*** conditions on the inner walls with outer walls insulated (the more practical representation for heat exchanger design) are higher than those of the other fundamental boundary conditions.

References

Anderson, D. A., Tannehill, J. C. and Pletcher, R. H. 1984. *Computational Fluid Mechanics and Heat Transfer*. Hemisphere, Bristol, PA

Capobianchi, M. and Irvine, T. F., Jr. 1992. Predictions of pressure drop and heat transfer in concentric annular ducts with modified power law fluids. *Wärme Stoffübertr.*, **27**, 209–215

Cheng, K. C. and Hwang, G. J. 1968. Laminar forced convection in eccentric annuli. *AIChE J.*, **14**, 510–512

Herwig, H. and Klemp, K. 1988. Variable property effects of fully developed laminar flow in concentric annuli. *J. Heat Transfer*, **110**, 314–320

Jonsson, V. K. and Sparrow, E. M. 1965. Results of laminar flow analysis and turbulent flow experiments for eccentric annular ducts. *AIChE J.*, **11**, 1143–1145

Kakaç, S., Shah, R. K. and Aung, W. 1987. *Handbook of Single-Phase Convective Heat Transfer*. Wiley, New York

Lundberg, R. E., McCuen, P. A. and Reynolds, W. C. 1963. Heat transfer in annular passages: Hydrodynamically developed laminar flow with arbitrarily prescribed wall temperatures or heat fluxes. *Int. J. Heat Mass Transfer*, **6**, 495–529

Manglik, R. M. and Bergles, A. E. 1994. Fully developed laminar heat transfer in circular-segment ducts with uniform wall temperature. *Num. Heat Transfer*, **26A**, 499–519

Manglik, R. M. and Bergles, A. E. 1991. Heat transfer enhancement in intube flows in process heat exchangers by means of twisted-tape inserts. Report No. HTL-8, Heat Transfer Laboratory, Rensselaer Polytechnic Institute, Troy, NY, December

Moghadam, H, and Aung, W. 1990. Numerical method for laminar convection in a concentric vertical annular duct with variable properties. *Num. Heat Transfer*, **18A**, 357–370

Piercy, N. A. V., Hooper, M. S. and Winny, H. F. 1933. Viscous flow pipes through pipes with cores. *London, Edinburgh, Dublin Philos. Mag. J. Sci.*, **15**, 647–676

Prusa, J. and Yao, L. S. 1983. Natural convection heat transfer between eccentric horizontal cylinders. *J. Heat Transfer*, **105**, 108–115

Prusa, J. and Yao, L. S. 1982. Numerical solution for fully developed flow in heated curved tubes. *J. Fluid Mech.*, **123**, 503–522.

Shah, R. K. and Bhatti, M. S. 1987. Laminar convective heat transfer in ducts. In *Handbook of Single-Phase Convective Heat Transfer*, S. Kakaç et al. (eds.), Wiley, New York, Ch. 3

Shah, R. K. and London, A. L. 1978. *Laminar flow forced convection in ducts*. Advances in Heat Transfer, Supple. 1, Academic Press, New York

Snyder, W. T. and Goldstein, G. A. 1965. An analysis of fully developed flow in an eccentric annulus. *AIChE J.*, **11**, 462–467

Suzuki, K., Szmyd, J. S. and Ohtsuka, H. 1991. Laminar forced convection heat transfer in eccentric annuli. *Heat Transfer—Jpn. Res.*, **20**, 169–183

Tiedt, W. 1966. Berechnung des laminaren und turbulenten reibungswiderstandes konzentrischer und exzentrisher ringspalte, Part I. *Chem. -Ztg., Chem. Appar.*, **90**, 813–821

Tiedt, W. 1967. Berechnung des laminaren und turbulenten reibungswiderstandes konzentrischer und exzentrisher ringspalte, Part II. *Chem. -Ztg., Chem. Appar.*, **91**, 17–25

Trombetta, M. L. 1971. Laminar forcec convection in eccentric annuli. *Int. J. Heat Mass Transfer*, **14**, 1161–1173